

ACS Nano. Author manuscript; available in PMC 2013 August 28.

Published in final edited form as:

ACS Nano. 2012 August 28; 6(8): 7281-7294. doi:10.1021/nn302393e.

# Gadolinium-Encapsulating Iron Oxide Nanoprobe as Activatable NMR/MRI Contrast Agent

Santimukul Santra<sup>†</sup>, Samuel D. Jativa<sup>†</sup>, Charalambos Kaittanis<sup>§</sup>, Guillaume Normand<sup>§</sup>, Jan Grimm<sup>§</sup>, and J. Manuel Perez<sup>†,\*</sup>

<sup>†</sup>Nanoscience Technology Center and Chemistry Department, University of Central Florida, 12424 Research Parkway, Suite 400, Orlando, FL 32826, USA

§Department of Radiology, Memorial Sloan Kettering Cancer Center, 1275 York Avenue, New York, NY 10065, USA

### **Abstract**

Herein we report a novel gadolinium-encapsulating iron oxide nanoparticle-based activatable NMR/MRI nanoprobe. In our design, Gd-DTPA is encapsulated within the polyacrylic acid (PAA) polymer coating of a superparamagnetic iron oxide nanoparticle (IO-PAA) yielding a composite magnetic nanoprobe (IO-PAA-Gd-DTPA) with quenched longitudinal spin-lattice magnetic relaxation ( $T_I$ ). Upon release of the Gd-DTPA complex from the nanoprobe's polymeric coating in acidic media, an increase in the  $T_I$  relaxation rate  $(1/T_I)$  of the composite magnetic nanoprobe was observed, indicating a dequenching of the nanoprobe with a corresponding increase in the  $T_{I}$ weighted MRI signal. When a folate-conjugated nanoprobe was incubated in HeLa cells, a cancer cell line overexpressing folate receptors, an increase in the  $1/T_I$  signal was observed. This result suggests that upon receptor-mediated internalization, the composite magnetic nanoprobe degraded within the cell's lysosome acidic (pH = 5.0) environment, resulting in an intracellular release of Gd-DTPA complex with subsequent  $T_I$  activation. No change in  $T_I$  was observed when the Gd-DTPA complex was chemically conjugated on the surface of the nanoparticle's polymeric coating or when encapsulated in the polymeric coating of a non-magnetic nanoparticle. These results confirmed that the observed  $(T_I)$  quenching of the composite magnetic nanoprobe is due to the encapsulation and close proximity of the Gd ion to the nanoparticles superparamagnetic iron oxide (IO) core. In addition, when an anticancer drug (Taxol) was co-encapsulated with the Gd-DTPA within the folate receptor targeting composite magnetic nanoprobe, the  $T_I$  activation of the probe coincide with the rate of drug release and corresponding cytotoxic effect in cell culture studies. Taken together, these results suggest that our activatable  $T_1$  nanoagent could be of great importance for the detection of acidic tumors and assessment of drug targeting and release by MRI.

### **Keywords**

Activatable MRI imaging; magnetic relaxation; iron oxide nanoprobe; Gd-DTPA complex; theranostic application

Magnetic resonance imaging (MRI) has become a powerful technique in the clinical diagnosis of disease and in animal imaging. <sup>1–4</sup> MRI is capable of obtaining tomographic images of living subjects with high spatial resolution as a result of perturbation of tissue

<sup>\*</sup>To whom correspondence should be addressed. J. Manuel Perez: Tel. 407-882-2843, Fax. 407-882-2819, jmperez@ucf.edu. Nanoscience Technology Center and Chemistry Department, University of Central Florida, 12424 Research Parkway, Suite 400, Orlando, FL 32826. USA.

water-protons in the presence of an external magnetic field.  $^{5-8}$ . MR contrast agents  $^{9-11}$  typically enhance contrast for more accurate diagnosis and most recently to allow for targeting imaging when a targeting ligand (*e.g.* antibody, peptide) is conjugated to the MR contrast agent.  $^{12,13}$  Among these agents, superparamagnetic nanoparticles  $^{14-16}$  and paramagnetic metal chelates are the most commonly used contrast agents.  $^{17-21}$  Superparamagnetic nanoparticles are typically composed of an iron oxide nanoparticle (IONP) surrounded by a polymeric coating to facilitate increased stability in aqueous media.  $^{22}$  They work by shortening the traverse relaxation time ( $T_2$  and  $T_2$ \*) of surrounding water protons, resulting in a decrease of the MR-signal (negative contrast, dark signal) on a  $T_2$ -weighted MRI sequence.  $^{23-28}$  On the other hand, paramagnetic gadolinium chelates create an increase in signal intensity on  $T_1$ -weighted images (positive contrast, bright signal) by shortening the longitudinal relaxation time ( $T_1$ ) of surrounding water protons.  $^{10,17,29-38}$ 

The development of an activatable MR imaging agent that reports on a biological process associated with diseases would greatly advance medical imaging of disease at a molecular level. <sup>39–41</sup> Activatable  $T_1$  or  $T_2$  agents, those that results in modulation of either the  $T_1$  or T2 relaxation time upon target binding, enzymatic activity or biological process associated with disease would be attractive MR imaging agents, resulting in high sensitivity and high signal to noise ratios with low background.  $^{20,42-48}$  Activatable Gd-based  $T_I$  agents have been previously described<sup>8,49,50</sup> and include those designed to be biologically activated by an enzyme such as  $\beta$ -Galactosidase<sup>51,52</sup> and  $\beta$ -Glucoronidase<sup>42,44</sup> as well as those activated by release of a drug. 53,54 However the lack of sufficient sensitivity and specificity as well as the hydrophobic nature of some of designed probes are major problems that hamper their implementation for clinical use. Activatable  $T_2$  IONP based agents are less common as it is often difficult to "quench" the strong superparamagnetic nature or magnetic moment of these nanoparticles. <sup>26–29,55</sup> Magnetic relaxation switches, have been developed based on IONP that cluster in the presence of a target or enzymatic activity leading to detectable changes in the  $T_2$  relaxation times. <sup>56–59</sup> However, the use of these  $T_2$  activatable agents has been difficult to implement in vivo and it has so far been limited to their use as nanosensors in molecular diagnostic applications. 57,60

An activatable  $T_1$  agent, one that can induce a faster  $T_1$  relaxation, would result in an increase in the  $T_I$ -weighted MR signal intensity upon target recognition for better diagnosis. Such an activatable agent could be beneficial in cancer diagnosis if it were designed to become activated upon tumor targeting, resulting in a brighter signal. Herein, we report the design, synthesis and characterization of a new dual mode MR contrast agent that becomes activated in an acidic environment, resulting in an increase in the  $T_T$ -weighted signal (brighter contrast). The designed MR agent is composed of superparamagnetic iron oxide nanoparticles that encapsulate Gd-DTPA chelates within the hydrophobic pockets of the nanoparticle's polyacrylic acid (PAA) coating (IO-PAA-Gd-DTPA). We hypothesized that the strong magnetic field induced by the large magnetic moment of the superparamagnetic iron oxide core will affect the relaxation process of the much weaker paramagnetic Gd-DTPA, resulting in quenching of its  $T_1$  signal (Scheme 1). The superparamagnetic iron oxide core is composed of thousands of iron (Fe<sup>+2</sup> and Fe<sup>+3</sup>) ions magnetically ordered within the nanocrystal in such a way that they collectively create a net magnetic moment larger than that of any single paramagnetic Fe<sup>+2</sup>/Fe<sup>+3</sup> or Gd<sup>+3</sup> ion. We then reasoned that the large magnetic moment of the iron oxide core would create a strong magnetic susceptibility in the proximity of the iron oxide core that will affect the T<sub>1</sub> relaxation of the Gd-DTPA encapsulated within the nanoparticle's polymeric coating. We observed that the  $T_1$  relaxation rate  $(1/T_I)$  of the Gd(III)-DTPA complex was quenched (OFF/Dark) when the Gd-DTPA complex was encapsulated within the PAA coating of the iron oxide nanoparticle (IO-PAA). Upon release of the quenched Gd-DTPA, an increase in the  $T_I$  relaxation rate was observed with marginal increase in the  $T_2$  relaxation rate (1/ $T_2$ ). This quenching effect is not observed

when the Gd chelate is attached to the surface of the IONP or when a non-magnetic nanoparticles, such as cerium oxide nanoparticles (NC-PAA), are used to encapsulate the Gd-DTPA. Corresponding  $r_1$  and  $r_2$  values for the IO-PAA-Gd-DTPA nanocomposite at different pH revealed a pH-dependent increase in the  $r_I$  of the nanocomposite suspension as the pH decreases, indicating  $T_I$  activation at acidic pH. The observed pH dependent increase in  $r_I$  was only observed when Gd-DTPA was encapsulated within the polymeric coating of the nanoparticle, but not when it was directly attached on the surface of the nanoparticle's polymeric coating. These results confirm that indeed the superparamagnetic iron oxide nanocrystal acts as a magnetic quencher for the Gd-DTPA T<sub>I</sub> only when the Gd-DTPA is encapsulated within the nanoparticle's polymeric coating in close proximity to the superparamagnetic core. Furthermore, when the IO-PAA-Gd-DTPA nanocomposite was conjugated with folic acid, its selective internalization and lysosomal localization within folate receptor positive cells allow for selective activation due to the lysosome's acidic pH. Finally, when the folate receptor targeting nanocomposite was used to co-encapsulate a cytotoxic drug (Taxol), dual delivery of the drug and  $T_I$  imaging activation was achieved. Therefore, our newly developed activatable nanoprobe (IO-PAA-Gd-DTPA) combines features of several important modalities, such as, (i) activatable  $T_I$ -weighted MRI contrast, (ii) T<sub>2</sub>-weighted MRI contrast, (iii) receptor-targeted internalization, and (iv) delivery of anticancer drug to tumors. These features make our magnetic nanoprobe as a potential MRactivatable contrast agent for cancer.

# **RESULTS and DISCUSSION**

# Synthesis and Characterization of Gd-DTPA Composite Iron Oxide Nanoparticles

Our IO-PAA-Gd-DTPA probe was synthesized by direct addition of Gd-DTPA during the course of the IO-PAA synthesis using a modified version of our previously published protocol.<sup>22</sup> In brief, an aqueous solution of PAA (0.45 mmol) and Gd-DTPA (0.04 mmol) was added and mixed thoroughly before addition of a mixture of iron salts (2.26 mmol of FeCl<sub>3</sub>.6H<sub>2</sub>O and 1.61 mmol of FeCl<sub>2</sub>.4H<sub>2</sub>O in dilute HCl solution) in aqueous ammonium hydroxide solution (0.05 M). The resulting dark-brown colored suspension of composite IO-PAA-Gd-DTPA nanoprobe was stirred for 1 h at room temperature and then centrifuged at 4000 rpm for 30 minutes to get rid of free polyacrylic acid, not encapsulated Gd-DTPA complex and other unreacted reagents. Finally, the composite nanoprobe suspension was purified using a magnetic column (Miltenyi Biotech) and washed with phosphate buffer saline (pH = 7.4) solution. This "in situ" encapsulation approach proved to be effective for the encapsulation of Gd-DTPA as no change in the size and relaxivity of the nanoprobes were found over the long period of time (Supporting Information, Table S1). The encapsulation of Gd-DTPA within the nanoprobe was confirmed by measuring the amount of Gd using ICP-MS (0.289 mg Gd/mL). The amount of Fe in the IO-PAA-Gd-DTPA preparation was determined as 2.0 mg Fe/mL, for a 0.05:1 Gd/Fe molar ratio. Magnetic relaxation measurements at 0.47 T of the composite nanoprobes resulted in a Gdconcentration based relaxivity of  $r_1 = 50.2 \pm 1.8 \text{ mM}^{-1}\text{Sec}^{-1}$  and  $r_2 = 87.3 \pm 2.4 \text{ mM}^{-1}\text{Sec}^{-1}$ ; and  $r_1 = 43.3 \pm 2.1 \text{ mM}^{-1}\text{Sec}^{-1}$  and  $r_2 = 230 \pm 3 \text{ mM}^{-1}\text{Sec}^{-1}$  based on Fe-concentration. These relatively high values for  $r_1$  and  $r_2$  might be due to the presence of both iron oxide and Gd(III) within the nanocomposite imaging probe and are comparable to reported values for high relaxivity probes. 35,40,41 Dynamic light scattering (DLS) studies indicated the presence of a stable and monodisperse suspension of nanoparticles with a hydrodynamic diameter of  $D = 79 \pm 2$  nm. The diameters of these magnetic nanoprobes were further confirmed by scanning transmittance electron microscopic (STEM) experiments, which show an average diameter of 80 nm (Supporting Information Figure S1). The synthesized IO-PAA-Gd-DTPA nanocomposite was found to be stable in PBS (pH = 7.4) and serum, as no binding, clustering or precipitations of the nanoparticles were observed over the long period of time. Similarly, the stability of the composite nanoparticles was further confirmed by observing

no significant changes in magnetic relaxations, as shown in Supporting Information Table S1. Taken together, these results indicate the effective encapsulation of Gd-DTPA into the IO-PAA polymeric matrix.

# pH-dependent activation of the Gd-DTPA Composite Magnetic Nanoprobes

We first evaluated the magnetic relaxation activation of the IO-PAA-Gd-DTPA nanoprobes in buffered solution within a pH range of 4.0 to 7.4. In these experiments, we measured the  $T_I$  and  $T_2$  of increasing concentrations of IO-PAA-Gd-DTPA nanoprobes at physiological (pH = 7.4) and acidic (pH = 4.0–6.0) buffered solutions.  $T_1$  and  $T_2$  readings were taken upon addition of the magnetic nanoprobes, immediately (0 h) and after a 24 h of incubation of the magnetic nanoprobes in the corresponding buffered solutions at 37 °C. First, we observed that the  $T_I$  relaxation rate  $(1/T_I)$  of the IO-PAA-Gd-DTPA nanoprobe (0 h, Figure 1A) was similar to that of the control IO-PAA nanoprobe (0 h, Supporting Information, Figure S2A) at all pH values (pH 4.0–7.4). This observation seems to indicate that in the IO-PAA-Gd-DTPA nanoprobe the  $1/T_I$  of Gd-DTPA was quenched upon encapsulation in the polymeric coating of IO-PAA. In contrast, we observed a greater increase in  $1/T_I$  of the IO-PAA-Gd-DTPA nanoprobe when incubated in acidic [pH =  $4.0 \, (\nabla)$ ,  $5.0 \, (\triangle)$  and  $6.0 \, (\bullet)$ ] buffered solution after 24 h (Figure 1B). However, no changes in  $1/T_I$  were observed either for IO-PAA-Gd-DTPA when incubated at physiological pH over the same 24 h time period (pH = 7.4, **\B**, Figure 1B) or for equivalent concentrations of control IO-PAA across the same pH values (pH = 4.0 to 7.4) after 24 h of incubation (Supporting Information, Figure S2B). These results suggest that the composite IO-PAA-Gd-DTPA nanoprobe gets activated, resulting in high  $\Delta 1/T_I$  numbers (Figure 1C) within 24 h of incubation in the acidic buffered solutions in contrast to values obtained with the control IO-PAA probe (Supporting Information, Figure S2C). In another set of experiments, minimal changes in  $T_2$  relaxation rate  $(\Delta 1/T_2)$  were observed for both the composite IO-PAA-Gd-DTPA nanoprobe (Figure 1D-F) and control IO-PAA nanoprobe (Supporting Information, Figure S2D-F) when incubated for 24 h in buffered solutions (pH = 4.0 to 7.4). These results indicated that the  $T_2$ of IO-PAA-Gd-DTPA probe was not quenched upon encapsulation of Gd-DTPA complex, as hypothesized. Taken together, the above results suggest that the inverse spin-lattice magnetic relaxation  $(1/T_I)$  of our composite IO-PAA-Gd-DTPA nanoprobes got activated when exposed to acidic environments, and could be of potential use as an activatable NMR/ MRI imaging agent for the detection of tumors, upon internalization and localization of the nanoprobes within lysosomes.

## pH-dependent studies of a Gd-DTPA cerium oxide nanocomposite as control studies

To confirm that the superparamagnetic nature of the iron oxide core is responsible for quenching the magnetic relaxation of the Gd-DTPA, we synthesized a PAA coated cerium oxide nanoparticle encapsulating Gd-DTPA (NC-PAA-Gd-DTPA). In this design, we selected a non-magnetic metal oxide core composed of cerium oxide (nanoceria, NC) to replace the magnetic iron oxide core during our synthesis protocol. We reasoned that incorporation of Gd-DTPA within the polymeric coating of a non-magnetic nanoparticle, such as cerium oxide will not result in T<sub>1</sub>-quenching or activation upon incubation in acidic media. The NC-PAA-Gd-DTPA nanoprobes were synthesized following a procedure similar to the one used to synthesize the IO-PAA-Gd-DTPA nanoprobe. Briefly, to a PAA solution in water, Gd-DTPA was added and mixed thoroughly before addition to a solution of cerium nitrate in ammonium hydroxide solutions. The synthesized NC-PAA-Gd-DTPA composite nanoprobe was purified using the SpectrumLab's Krosflo filtration system. DLS and ICP-MS of the nanoprobe aqueous suspension indicated the presence of 88±1 nm nanoparticles with a Gd concentration of 0.315 mg/mL (Supporting Information, Scheme S1). These values were similar to those obtained for the IO-PAA-Gd-DTPA nanoprobes, suggesting that the size, polymer coating thickness and amount of encapsulated Gd was similar in both

preparations. Magnetic relaxation values of the aqueous nanoparticle suspension revealed an  $r_1 = 34.3 \pm 2.1 \text{ mM}^{-1}\text{Sec}^{-1}$  and  $r_2 = 60 \pm 5.2 \text{ mM}^{-1}\text{Sec}^{-1}$  (based on Gd concentration), further confirming the successful encapsulation of Gd in the nanoparticle's polymeric core. The magnetic relaxation rates 1/T<sub>1</sub> and 1/T<sub>2</sub> of the NC-PAA-Gd-DTPA nanoprobes indicated no change in  $\Delta 1/T_I$  (Figure 2C) before (0 h, Figure 2A) or after 24 h incubation (Figure 2B) in either physiological (pH = 7.4) or acidic (pH = 4.0) buffered solutions, indicating no magnetic relaxation activation at acidic pH. Similarly, no changes in  $T_2(\Delta 1/T_2$ , Figure 2D-F) were recorded for the NC-PAA-Gd-DTPA nanoprobes, and as expected no changes in magnetic relaxation rates  $(1/T_1)$  and  $1/T_2$  were observed in the case of non-magnetic nanoceria control probe NC-PAA<sup>61,62</sup> (Supporting Information, Figure S3). Taken together, the above results suggest that the observed quenching of the Gd-DTPA  $T_1$  relaxation rate (1/  $T_{I}$ ) only occurred when the Gd-DTPA was encapsulated in close proximity to a superparamagnetic core (iron oxide) and not when encapsulated within the polymeric coating of a non-magnetic core. These data also suggests that the observed quenching is not due to immobilization of the Gd-DTPA within a polymer matrix surrounding a nonmagnetic core (cerium oxide). In another set of experiments, no significant pH-dependent activation was observed when an iron oxide nanocomposite containing Ca-DTPA instead of Gd-DTPA was used, further indicating that the release of the paramagnetic Gd-chelate is responsible for the observed activation in acidic pH (Supporting Information, Figure S4). Taking together, these results indicate that the observed pH-dependent T<sub>1</sub>-activation observed with our IO-PAA-Gd-DTPA nanocomposite is due to quenching of the T<sub>1</sub> relaxativity of the Gd-DPTA chelate when in close proximity to the iron oxide core and subsequent activation upon release from the nanoparticle's polymeric coating.

### Magnetic Relaxations of the Gd-DTPA Surface Conjugating Magnetic Nanoprobes

In our hypothesis, we stated that the close proximity of Gd (a weak paramagnetic ion) within the polymeric matrix of iron oxide nanoparticles (a strong superparamagnetic nanocrystal) affects the T<sub>1</sub> relaxation of Gd. If our hypothesis is correct, conjugation of a Gd-DTPA directly on the nanoparticle's surface will not result in quenching of the  $T_I$  values. In this case, the Gd-DTPA will be further away from the iron oxide core and its T<sub>1</sub> relaxation will be less affected by the strong magnetic susceptibility of the magnetic core. To further test this hypothesis, we then synthesize a IO-PAA-Gd-DTPA magnetic nanoprobe where the Gd-DTPA was conjugated directly on the IO-PAA surface carboxylic acid groups (Supporting Information, Scheme S2). Briefly, IO-PAA was first conjugated with ethylenediamine using the water-soluble carbodiimide chemistry, as previously described.<sup>22</sup> The resulting aminated IO-PAA was then conjugated with Gd(III) chelated 2-(4isothiocyanatobenzyl)-diethylenetriaminepentaacetic acid (p-SCN-Bn-Gd-DTPA) in basic PBS buffer (pH = 8.4). The conjugated magnetic nanoprobe was purified using small magnetic columns (Miltenyi Biotech) and washed with PBS (pH = 7.4), prior to characterizations and magnetic relaxation measurements. The successful conjugation of the functional Gd-DTPA complex was confirmed by performing ICP-MS experiments and the resulting Gd concentration was found to be 0.201 mg/mL. The amount of Fe in the preparation was determined as 2.0 mg Fe/mL, for a 0.04:1 Gd/Fe molar ratio. The magnetic relaxation values of the conjugated nanoprobe was  $r_1 = 63.4 \pm 1.5 \text{ mM}^{-1}\text{Sec}^{-1}$  and  $r_2 =$ 92.1 $\pm$ 3.8 mM<sup>-1</sup>Sec<sup>-1</sup> (based on Gd concentration); and  $r_1 = 49.9 \pm 1.3$  mM<sup>-1</sup>Sec<sup>-1</sup> and  $r_2 =$ 243±3 mM<sup>-1</sup>Sec<sup>-1</sup>(based on Fe concentration). The  $T_1$  and  $T_2$  relaxation rates (1/ $T_1$  and 1/  $T_2$ ) of the nanoprobe were measured in a similar fashion as described earlier and results compared to those of the control IO-PAA nanoprobe. Results showed no change in  $\Delta 1/T_1$ (Figure 3C) before (0 h, Figure 3A) or after (24 h, Figure 3B) incubating in various buffered solutions and were found to be similar to that of control IO-PAA probe with no magnetic activation (Supporting Information, Figure S2). Similarly, no changes in spin-spin relaxations ( $\Delta 1/T_2$ , Figure 3D–F) were observed after the 24 h of treatment. Overall, the

above results indicate that the encapsulation of the Gd-DTPA within the polymeric coating and close proximity to the iron oxide core responsible for the Gd relaxation quenching, which was then activated upon release.

Meanwhile, the  $r_I$  and  $r_2$  relaxation values based on Gd concentrations of the IO-PAA-Gd-DTPA nanoprobes indicate a significant pH-dependent increase in the  $r_I$  of the nanoprobes when the Gd is encapsulated within the polymeric coating of the iron oxide nanoparticles (Table 1). Results show that by decreasing the pH of the solution to a mildly acidic condition (pH 6.0), a significant percent increase of 44% in the Gd-based  $r_I$  is observed. This value contrast with a small increase of 5% observed when the Gd is conjugated on the nanoparticle surface, further indicating that indeed encapsulation within the nanoparticle's polymeric matrix is essential for the observed  $T_I$  activation. The observed increase in  $r_I$  is larger at higher pH, observing a 68% increasing at pH 5.0, the typical pH within lysosomes. Even though pH-dependent percent changes in  $r_2$  are also observed in the Gd encapsulated nanocomposite, they are not as large as the values obtained with  $r_I$ . Taken together, these results confirm the  $T_I$  activation of the IO-PAA-Gd-DTPA nanoprobes upon decreases in pH, particularly within the range (pH 6-5) observed within lysosomes.

# MRI-Based T<sub>1</sub>-Weighted Activation of the Composite IO-PAA-Gd-DTPA Nanoprobe

Next, we investigated if the observed pH-dependent increases in  $r_1$  of the IO-PAA-Gd-DTPA nanoprobe result in increases in the  $T_t$ -weighted signal by MRI, leading to an increase in the brightness of the image. For these experiments, the  $T_T$  and  $T_Z$  weighted MR images (MRI, B = 4.7 T) of nanoprobe solutions at pH 5.0 were acquired immediately (Figure 4A1) and after a 24 h incubation (Figure 4A2) in the pH 5.0 buffer. An increase in the  $T_I$ -weighted MR signals was observed as the concentration of the activatable IO-PAA-Gd-DTPA nanoprobes increased (from 0.06 µM to 2.4 µM of Gd), resulting in an increase in the signal of the corresponding MR images (Figure 4A2). The observed signal increase after a 24 h incubation in the pH 5.0 buffer corresponded to an increase in the  $(1/T_I)$ relaxation rate ( $\triangle$ , Figure 4C). As expected, a minimal increase in  $T_2$ -weighted MR signals (T2 Map, Figure 4B) or corresponding inverse spin-spin magnetic relaxations ( $1/T_2$ , Figure 4D) were observed from the IO-PAA-Gd-DTPA nanoprobes due to the absence of any  $T_2$ activation. However, in this case the MR signals were found to be decreased, since the iron concentrations increased with the rising nanoprobe concentrations. The calculated  $r_1$  and  $r_2$ values at 4.7 T for the IO-PAA-Gd-DTPA nanoprobe before and after a 24 h incubation at pH 5.0 also show an increase in  $r_1$  values (24.8±1.2 vs 45.2±1.9 mM<sup>-1</sup>Sec<sup>-1</sup>), for a percent increase in  $r_1$  of 87 %. Meanwhile, a modest increase in  $r_2$  was observed as (75.4±2.3 vs 91.5±3.1 mM<sup>-1</sup>Sec<sup>-1</sup>) for a percent increase of only 21%. In another set of experiments, no change in the MR signals (both T1- and T2-Map) or corresponding magnetic relaxations were observed due to the absence of any magnetic activation from our control IO-PAA probe (Supporting Information, Figure S5). Taken together, the above results confirm that our activatable IO-PAA-Gd-DTPA nanoprobes get activated at acidic pH, and activation was indicated by the increase in the  $T_t$ -weighted MRI signal. These results also suggest the potential diagnostic applications of our novel NMR/MRI activatable composite iron oxide nanoprobes.

#### In Vitro Activation of the Composite IO-PAA-Gd-DTPA Nanoprobe

To evaluate the potential biomedical applications of the activatable IO-PAA-Gd-DTPA nanoprobes, we assessed their magnetic activations using cultured cells. We hypothesized that upon receptor mediated endocytosis, the nanoparticles will localize in acidic lysosomes, therefore becoming activated as the encapsulated Gd-DTPA complex gets released at lower pH. For these experiments, the magnetic nanoprobes were functionalized with folic acid, following published protocols, <sup>22,63</sup> in order to assess their targeted imaging capabilities

towards folate receptor (FR)-expressing cancer cells. We hypothesized that upon internalization into FR expressing cancer cells, T<sub>I</sub> activation of the composite IO-PAA-Gd-DTPA-Fol nanoprobe would be triggered by the lysosomal acidic environment (pH = 5.0), resulting in vitro activation of the MRI signals. In these experiments, we used a FR positive human cervical carcinoma cell line (HeLa cells, 10,000 cells/well) and as negative control we used H9c2 cardiomyocyte (10,000 cells/well) that do not express FR. Cells were incubated with the nanoprobes (100 µL, 28 mM) at different time-points, trypsinized, centrifuged and resuspended in PBS (pH = 7.4) before measuring  $T_1$  and  $T_2$  of the nanoparticle cell suspension. As hypothesized, compared to the control IO-PAA-Fol nanoprobes, significant activation in inverse spin-lattice magnetic relaxations  $(1/T_I)$  was observed in HeLa cells incubated with the activatable IO-PAA-Gd-DTPA-Fol nanoprobes ( $\bullet$ , Figure 5A). While, no significant changes in  $1/T_2$  were observed from HeLa cells incubated with either of the probes (Figure 5B). These results further supported the in vitro activatable MR imaging capability of the composite nanoprobes, whereas the control probe's (, IO-PAA-Fol) magnetic relaxation remained unchanged after the FR-mediated internalizations. In contrast, no significant changes in magnetic relaxations (both  $1/T_I$  and  $1/T_I$ )  $T_2$ ) were observed from H9c2 cells (FR negative) incubated with either one of the nanoprobes, suggested the lack of any receptor-mediated internalizations of our magnetic nanoprobes (Figure 5C and 5D). Furthermore, control experiments using HeLa cells preincubated with excess folic acid (0.2 mg/ml) in the culturing media resulted in abrogation of the pH-dependent 1/T1 activation (Supporting Information, Figure S6). Taken together, our results confirm that the FR-mediated internalizations and lysosomal acidic pH-assisted release of the encapsulating Gd-DTPA complex was responsible for the enhanced MR signal from our composite IO-PAA-Gd-DTPA-Fol nanoprobe. These results also indicate that the activatable MR imaging capability of our composite nanoprobe could potentially be useful in the detection and treatment of cancer in clinical settings.

# pH-dependent dual release of the Gd-DTPA complex and Taxol

Previously, we have reported the encapsulation and release of a cytotoxic drug (Taxol) from the polymeric coating of iron oxide nanoparticles as a theranostic nanoagent for the potential treatment of cancer. 22 We then hypothesized whether we could encapsulate both Taxol and Gd-DTPA, within the same nanoparticle creating a dual therapeutic and activatable magnetic nanoprobe. The IO-PAA-Gd-DTPA nanoprobes were then used to encapsulate Taxol as previously described using the solvent diffusion method. <sup>22,63</sup> Briefly, to a suspension of IO-PAA-Gd-DTPA nanoprobes (2.5 mL, 28 mmol) in PBS, the dimethyl sulfoxide (DMSO) solution of Taxol (10  $\mu$ L, 0.5  $\mu$ g/ $\mu$ L) was added drop-wise at room temperature. The resulting purified IO-PAA-Gd-DTPA-Taxol nanoparticles were characterized by measuring their size using DLS ( $D = 84\pm2$  nm), taxol encapsulation efficiency (EE) =  $52\pm2.4$  % using HPLC ( $\lambda_{abs}$  = 227 nm) and calculating the Gd concentration (0.215 mg/mL) by performing ICP-MS experiments. To evaluate the dual release of Taxol and Gd, the IO-PAA-Gd-DTPA-Taxol nanoprobe were incubated in a pH 5.0 buffered PBS solutions and the rate of release of the drug and Gd was accessed using a dynamic dialysis technique. Briefly, the IO-PAA-Gd-DTPA-Taxol nanoprobes (50 µL, 28 mM) were taken in a small dialysis cup (MWCO 6-8KDa) and incubated in PBS buffer (pH = 5.0) solution at 37 °C. The rate of release of taxol and Gd was monitored by collecting aliquots from the outside reservoir buffer and measuring the amount of released taxol via HPLC experiment ( $\lambda_{abs} = 227$  nm) and Gd by measuring the increase in  $T_I$  relaxation rate with time. Results showed, a time dependent increase in the amount of Taxol (▲, Figure 6A) and Gd-DTPA (▼, Figure 6B) released upon incubation at pH 5.0. These results suggest that indeed the acid-mediated degradation and/or swelling of the PAA coatings results in the simultaneous release of both Taxol and Gd. Interestingly, a slower rate of Gd-DTPA release from the nanoprobe is observed in contrast to Taxol, this could be due to a possible higher

extend of hydrogen bonding between Gd-DTPA and the carboxylic groups within the polymeric coating internal cavities surrounding the iron oxide core. In contrast, when similar experiments were performed at physiological pH (PBS, pH = 7.4, 37 °C), no significant release of Taxol ( $\blacksquare$ , Figure 6A) or Gd was observed ( $\bullet$ , Figure 6B). Similarly, no significant release of Taxol or increase in magnetic relaxations ( $1/T_I$ ) was observed when the IO-PAA-Gd-DTPA-Taxol nanoprobe was incubated in serum at 37 °C (Supporting Information, Figure S7). These findings indicate that the IO-PAA-Gd-DTPA-Taxol nanoprobe is stable at neutral pH and physiological conditions, only releasing its cargo (Taxol and Gd) in an acidic environment.

### In Vitro cytotoxicity of taxol-encapsulating activatable IO-PAA-Gd-DTPA nanoprobes

Finally, we examined the differential in vitro cytotoxicity of the functionalized magnetic nanoprobes (35 μL, 28 mM in PBS pH = 7.4) using FR expressing human cervical cancer cells (HeLa, 2500 cells/well) and FR negative cardiomyocyte cell lines (H9c2, 2500 cells/ well). Results confirmed a time-dependent decrease in the number of viable HeLa cells, when incubated with folate-decorated IO-PAA-Gd-DTPA-Taxol nanoprobes 5 (Figure 7A), showing more than 90% reduction in cell viability after 24 h of incubation. However, the folate-decorated IO-PAA-Gd-DTPA nanoprobes showed nominal toxicity (4) and comparable with the IO-PAA-Fol (1) lacking Gd-DTPA complex, as published earlier. <sup>22</sup> As expected, nominal cytotoxicity was observed when HeLa cells were incubated with the IO-PAA-Gd-DTPA (2) and IO-PAA-Gd-DTPA-Taxol (3), due to absence of any receptormediated internalizations. These results suggest that the cytotoxicity of the nanoprobes was not affected by the encapsulation of Gd due to the presence of PAA polymer coatings. In addition, no significant reduction in cell viability was observed when H9c2 cells, which do not overexpress FR, were incubated with all the functional magnetic nanoprobes (Figure 7B), suggesting biocompatibility and potential applications of our nanoprobes for the targeted imaging and treatment of cancers. Taken together, the above results suggest that our folate-decorated activatable IONP-PAA-Gd-DTPA-Taxol nanoprobe can detect tumors using MR imaging, while targeting and delivering a chemotherapeutic agent (Taxol) via folate receptors.

# **CONCLUSION**

In summary, we report an activatable Gd-DTPA-encapsulating iron oxide NMR/MRI nanoprobe, with quenched longitudinal (spin-lattice) magnetic relaxation  $(T_1)$  of the encapsulated Gd-DTPA (low  $1/T_1$ ) by the iron oxide nanoparticles. In our design, the  $T_1$ relaxation of the Gd-DTPA complex becomes activated (de-quenched), resulting in higher 1/  $T_I$  values and enhanced  $T_I$ -weighted MRI contrast, upon acid-mediated degradation and release of the  $T_I$  agent. Our results clearly indicated that the magnetic relaxation of the Gd-DTPA chelate (T1 agent) is quenched as a result of such encapsulation, whereas the transverse (spin-spin) magnetic relaxation (T2) of iron oxide was minimally affected. Our results also demonstrated that the folate receptor-mediated internalization and the subsequent lysosomal localization induced an intracellular release of Gd-DTPA complex, resulting in an enhanced  $1/T_I$  signal. In addition, when a Taxol-encapsulating activatable magnetic nanoprobes was used, the intracellular drug's release was monitored by the observed changes in 1/T1. The presence of folate on the activatable magnetic nanoprobe guarantees a selective activation and release of the drug only in folate-receptor positive cells, minimizing toxicity to healthy cells. In contrast, no  $T_1$  activation is observed in the Gd-DTPA surface-conjugated IONPs or Gd-DTPA encapsulating non-magnetic NC-PAA, confirming that quenching was due to the close residence of the Gd-DTPA to the superparamagnetic iron oxide (IO) core and not due to the presence of any non-magnetic metallic core (cerium oxide) or polymeric (PAA) coatings. Overall, the pH-dependent and

targeted activation upon cellular internalization of our designed IO-PAA-Gd-DTPA nanoprobe are important attributes of this novel platform technology that can be further developed into others MR-activatable and theranostic nanoprobes.

# **MATERIALS AND METHODS**

#### **Materials**

Iron salts: ferrous(II) chloride tetrahydrate (FeCl<sub>2</sub>.4H<sub>2</sub>O) and ferric(III) chloride hexahydrate (FeCl<sub>3</sub>.6H<sub>2</sub>O), gadolinium(III) chloride hexahydrate (GdCl<sub>3</sub>.6H<sub>2</sub>O), cerium(III) nitrate hexahydrate (CeNO<sub>3</sub>.6H<sub>2</sub>O), diethylenetriaminepentaacetic acid (DTPA), ammonium hydroxide, hydrochloric acid, sodium hydroxide, chloropropryl amine, sodium azide, copper(I) iodide, ethylenediamine (EDA), folic acid, *N*,*N*-dimethylformamide (DMF), dimethyl sulfoxide (DMSO), 3-(4,5-dimethylthiazol-2-yl)-2,5-diphenyltetrazolium bromide (MTT), *N*-hydroxysuccinimide (NHS), 2-(*N*-morpholino) ethanesulfonic acid (MES), polyacrylic acid (PAA) and other chemicals were purchased from Sigma-Aldrich. 2-(4-isothiocyanatobenzyl)-diethylenetriaminepentaacetic acid [*p*-SCN-Bn-DTPA] was purchased from Macrocyclics. EDC [1-Ethyl-3-(3-dimethylaminopropyl) carbodiimide hydrochloride] was obtained from Pierce Biotechnology. The human cervical carcinoma (HeLa) and cardiomyocyte (H9c2) cell lines were obtained from ATCC. Magnetic columns (LS Column) were purchased from Miltenyi Biotech for the purification of magnetic nanoprobes using QuadroMACS separators. Dialysis membranes were obtained from Spectrum Laboratories. Nitrogen purged DI water was used in all synthesis.

### Synthesis of the Gd-DTPA complexes

Chelation of the rare-earth element Gadolinium (Gd) with diethylenetriaminepentaacetic acid (DTPA) or with functional DTPA, p-SCN-Bn-DTPA [2-(4-isothiocyanatobenzyl)-diethylenetriaminepentaacetic acid] results in a strongly paramagnetic, stable complex that is well tolerated in animals. These complexes were synthesized following the literature reported method. <sup>64,65</sup> Briefly, a solution of GdCl<sub>3</sub>.6H<sub>2</sub>O (4.49 g, 0.0121 mol) in H<sub>2</sub>O (10 mL) was added drop-wise to a solution of DTPA (5.0 g, 0.0127 mol) or p-SCN-Bn-DTPA (0.0127 mol) in H<sub>2</sub>O (30 mL) containing 2N NaOH (5.0 mL) solution. The pH of the final reaction mixture was maintained at pH 6.8 by constant addition of 2N NaOH solution. The reaction was continued at 80 °C for 12 h before concentrated to 20 mL. The observed white crystals were dissolved in minimum amount of water before precipitating in ethanol. The precipitate was filtered and dried under vacuum to obtain the Gd(III) complex as a white solid (Yield: 86%).

# Synthesis of the Gd-DTPA-encapsulating composite iron oxide nanoprobes (IO-PAA-Gd-DTPA)

For the synthesis of Gd-DTPA-encapsulating composite nanoprobe (IO-PAA-Gd-DTPA), we used a novel water-based, 'in situ' encapsulation approach for the successful encapsulation of Gd-DTPA complex. In this approach, three different solutions were prepared; an *iron salt solution* [0.61 g of FeCl<sub>3</sub>. 6H<sub>2</sub>O and 0.32 g of FeCl<sub>2</sub>. 4H<sub>2</sub>O in dilute HCl solution (100 µL of 12 N HCl in 2.0 mL H<sub>2</sub>O)]; an *alkaline solution* [1.8 mL of 30 % NH<sub>4</sub>OH solution in 15 mL of N<sub>2</sub> purged DI water]; and a *paramagnetic stabilizing solution* [800 mg of PAA and 20 mg of Gd-DTPA complex in 5 mL of DI water]. To synthesize the composite IO-PAA-Gd-DTPA nanoprobe, the *iron salt solution* was added to the *alkaline solution* under vigorous stirring. The resulting dark suspension of iron oxide nanoparticles was stirred for 10 seconds before addition of the *paramagnetic stabilizing solution* and stirred for 1 h. The resulting suspension of composite IO-PAA-Gd-DTPA nanoprobe was then centrifuged at 4000 rpm for 30 minutes to get rid of free polyacrylic acid, Gd-DTPA complex and other unreacted reagents. Finally, the composite IO-PAA-Gd-DTPA nanoprobe

suspension was purified using magnetic columns and washed with phosphate buffer saline (pH = 7.4) solution. The iron concentration and magnetic relaxation of the PAA-IONPs was determined as previously reported. The successful coating of the IONPs with PAA was confirmed by the presence of a negative zeta-potential ( $\zeta$  = -41 mV) and the characteristic acid carbonyl band on the FT-IR spectroscopic analysis of the nanoparticles (Supporting Information, Figure S1).

# Synthesis of the theranostic cargos-encapsulating composite activatable magnetic nanoprobes

Taxol was encapsulated in the PAA polymer coating of magnetic nanoprobe, following the previously reported solvent diffusion method.  $^{22,66}$  Briefly, to a suspension of IO-PAA-Gd-DTPA nanoprobes (2.5 mL, 28 mmol) in PBS, a dimethyl sulfoxide (DMSO) solution of Taxol (10  $\mu$ L, 0.5  $\mu$ g/ $\mu$ L) was added drop-wise at room temperature with continuous stirring at 1000 rpm. The taxol-encapsulating nanoprobes (IO-PAA-Gd-DTPA-Taxol) were purified using magnetic column (Miltenyi Biotech) and then dialyzed (using 6–8K MWCO dialysis bag) three times against deionized water and finally against phosphate buffered saline solution. The resulting IO-PAA-Gd-DTPA-Taxol nanoparticles were characterized by measuring their size using DLS ( $D=84\pm2$  nm), the taxol encapsulation efficiency (EE) =  $52\pm2.4$  % using HPLC ( $\lambda_{abs}=227$  nm).

# Synthesis of folate-decorated magnetic nanoprobes: Click chemistry

To synthesize folate-decorated functional IO-PAA nanoprobes, the surface carboxylic acid groups of the nanoprobes were alkynated using propargylamine as a reagent and the water-based carbodiimide chemistry was followed as previously reported. The resulting alkynated IO-PAA nanoprobes were purified using magnetic columns. The highly specific "click" chemistry was used to conjugate an azide-functionalized folic acid with the purified alkynated IO-PAA, as described in the previously reported methods.  $^{22,67}$  Briefly, the alkynated IO-PAA (4.0  $\times$  10 $^{-3}$  mmol) in bicarbonate buffer (pH = 8.5) were taken to an eppendorf tube containing catalytic amount of CuI (5.0  $\times$  10 $^{-10}$  mmol) in 250  $\mu$ L of bicarbonate buffer (pH= 8.5) and vortexed. To the resulting solution, the azidefunctionalized folic acid  $^{22,63}$  (8.0  $\times$  10 $^{-2}$  mmol) in DMSO was added and the reaction was incubated at room temperature for 12 h. The synthesized folate-decorated IO-PAA was purified using the magnetic column and finally washed using PBS solution (pH = 7.4). The folate-decorate IO-PAA was stored in refrigerator for further characterization.

### Synthesis of the Gd-DTPA-encapsulating composite nanoceria (NC-PAA-Gd-DTPA)

For the synthesis of Gd-DTPA-encapsulating composite nanoceria, we have modified our previously reported stepwise method and followed the 'in situ' encapsulation approach. In this approach, 1M cerium(III) nitrate (2.17 g in 5.0 mL of water) solution was added to 30.0 mL of ammonium hydroxide solution (30% w/v) under continuous stirring at room temperature. Then, after 45 seconds of stirring, an aqueous mixture containing the PAA polymer and Gd-DTPA complex (800 mg of PAA and 20 mg of Gd-DTPA in 5 mL of water) was added and allowed to stir for 3 h at room temperature. The preparation was then centrifuged at 4000 rpm for two 30 minute cycles to settle down any debris and large agglomerates. The supernatant solution was then purified from free PAA, Gd-DTPA complex or other chemicals and concentrated using SpectrumLab's KrosFlo filtration system.

# Synthesis of the Gd-DTPA surface conjugating magnetic nanoprobes (IO-PAA-Gd-DTPA-Surface)

The polyacrylic acid coated iron oxide nanoparticles (IO-PAA) were synthesized using our previously reported alkaline precipitation method.<sup>22</sup> Briefly, a Fe<sup>+3</sup> /Fe<sup>+2</sup> solution in water was rapidly mixed with an ammonium hydroxide solution for 30 seconds, prior to addition of the PAA polymer solution in water. The synthesized IO-PAA were purified using magnetic columns to remove any unreacted reagents and phosphate buffered saline (PBS, pH 7.4) was used as running solvent. To incorporate amine groups to the nanoparticles, ethylenediamine was used as an aminating agent and the water-based carbodiimide chemistry (using EDC and NHS reagents) was followed, as previously reported.<sup>22,62</sup> The successful amination of the IO-PAA nanoparticles were confirmed by measuring their overall positive surface charge (zeta potential  $\zeta = +15 \text{ mV}$ ) using Malvern's Zetasizer. To synthesize the Gd-DTPA surface conjugating IO-PAA nanoprobe, the aminated IO-PAA was reacted with the isothiocyanate group of the p-SCN-Bn-DTPA chelated with GdCl<sub>3</sub>.6H<sub>2</sub>O salt. In a typical reaction, the isothiocyanate functional Gd-DTPA chelate (p-SCN-Bn-Gd-DTPA, 25 mmol) was added to the aminated IO-PAA nanoprobe (1 mmol) in the presence of basic phosphate buffered saline (PBS, pH 8.4) and incubated overnight at room temperature. The resulting Gd-DTPA surface conjugating IO-PAA nanoprobe was purified using small magnetic columns (Miltenyi Biotech) and washed with phosphate buffered saline (PBS, pH = 7.4), prior to characterizations and magnetic relaxation measurements.

# Measurement of the hydrodynamic diameter and surface zeta potential of the functional IO-PAA

The size and dispersity of the synthesized composite IO-PAA was measured using dynamic light scattering (DLS) PDDLS/CoolBatch 40T instrument with Precision Deconvolve 32 software. The overall surface charges (zeta potential) of this functional IO-PAA were measured using a Zetasizer Nano ZS from Malvern Instruments. These experiments were performed by placing 10  $\mu L$  of the composite magnetic nanoprobes in 990  $\mu L$  of distilled water. All measurements were performed in triplicate.

### Measurement of magnetic relaxations

Magnetic relaxation measurements were conducted with a compact magnetic relaxometer (0.47 T mq20, Bruker), by taking composite magnetic nanoprobes with various concentrations. Magnetic resonance imaging (MRI) of the magnetic phantoms was achieved using the MRI/MRS facility utilizing a 4.7 T 33-cm bore magnet imaging/spectroscopy system (MSKCC, New York). All measurements were performed in triplicate.

# **HPLC** experiment

HPLC experiments were carried out using PerkinElmer's Series 200 instrument to study drug release kinetics. In a typical experiment, upon addition of acidic PBS solution (pH = 5.0) to the taxol-encapsulating IO-PAA-Gd-DTPA (50  $\mu L$ , 28 mM), the rate of release of encapsulating taxol was monitored in a timely manner at 37 °C using HPLC ( $\lambda_{abs}$  = 227 nm) chromatography.

# **Cell cultures**

The human cervical cancer (HeLa) and cardiomyocyte (H9c2) cells were obtained from ATCC, and maintained in accordance to the supplier's protocols. Briefly, the cervical cancer cells were grown in a 5% FBS-containing DMEM medium supplemented with L-glutamine, streptomycin, amphotericin B and sodium bicarbonate. The H9c2 cells were propagated in a 10% FBS-containing MEM medium containing penicillin, streptomycin and bovine insulin

(0.01 mg/mL). Cells were grown in a humidified incubator at 37  $^{\circ}\text{C}$  under 5%  $\text{CO}_2$  atmosphere.

### In Vitro magnetic activations of the composite nanoprobes

The human cells (HeLa and H9c2, 10,000 cells/well) were incubated with the folate-decorated activatable IO-PAA-Gd-DTPA-Fol nanoprobe and the control IO-PAA-Fol nanoprobe (100  $\mu$ L, 28 mM) at different incubation times. The cells were then trypsinized and centrifuged. The resulting cell pellet was suspended in phosphate buffer saline (PBS, pH = 7.4) and magnetic relaxations of these solutions were measured using the bench-top magnetic relaxometer (B = 0.47 T mq 20) from Bruker. All measurements were performed in triplicate.

# Cytotoxicity assay

H9c2 and HeLa cells (2,500 cells/well) were seeded in 96-well plates, incubated with the corresponding composite IO-PAA nanoprobes (35  $\mu L$ , 28 mM in PBS pH = 7.4) at 37 °C. After the specific time incubation, each well was washed three times with 1X PBS and treated with 30  $\mu L$  MTT (2  $\mu g/\mu L$ ) for 2 h. The resulting formazan crystals were dissolved in acidic isopropanol (0.1 N HCl) and the absorbance was recorded at 570 and 750 nm (background), using a Synergy  $\mu Quant$  microtiter plate reader (Biotek). Experiments were performed in triplicate.

### ASSOCIATED CONTENT

Supporting Information Available: Detailed physical characterizations of the magnetic probes including dynamic light scattering (DLS), scanning transmittance electron microscopy (STEM), FT-IR, zeta potential, stability of the nanoprobes at different conditions, MRI-based magnetic relaxations, encapsulating drug release and cytotoxicity studies. This material is available free of charge *via* the Internet at http://pubs.acs.org.

# **Supplementary Material**

Refer to Web version on PubMed Central for supplementary material.

## **Acknowledgments**

This work was supported in part by NIH Grant GM084331 and UCF-NSTC Start Up Fund, all to J.M.P. We thank Dr. S. M. Hussain from the US Air Force's Wright-Patterson Air Force Base, Ohio, USA for assistance with ICP-MS experiments.

### References

- Winter PM, Caruthers SD, Wickline SA, Lanza GM. Molecular Imaging by MRI. Curr Cardio Reports. 2006; 8:65–69.
- 2. Hu X, Norris DG. Advances in High-Field Magnetic Resonance Imaging. Ann Rev Biomed Eng. 2004; 6:157–184. [PubMed: 15255766]
- 3. Aime S, Cabella C, Colombatto S, Geninatti Crich S, Gianolio E, Maggioni F. Insights into the Use of Paramagnetic Gd(III) Complexes in MR-Molecular Imaging Investigations. J Magn Reson Imaging. 2002; 16:394–406. [PubMed: 12353255]
- 4. Louie A. Multimodality Imaging Probes: Design and Challenges. Chem Rev. 2010; 110:3146–3195. [PubMed: 20225900]
- Mulder WJ, Strijkers GJ, Griffioen AW, van Bloois L, Molema G, Storm G, Koning GA, Nicolay K. A Liposomal System for Contrast-Enhanced Magnetic Resonance Imaging of Molecular Targets. Bioconjugate Chem. 2004; 15:799–806.

 Mazooz G, Mehlman T, Lai TS, Greenberg CS, Dewhirst MW, Neeman M. Development of Magnetic Resonance Imaging Contrast Material for *In Vivo* Mapping of Tissue Transglutaminase Activity. Cancer Res. 2005; 65:1369–1375. [PubMed: 15735023]

- 7. Josephson L, Tung CH, Moore A, Weissleder R. High-Efficiency Intracellular Magnetic Labeling With Novel Superparamagnetic-Tat Peptide Conjugates. Bioconjugate Chem. 1999; 10:186–191.
- 8. Caravan P, Ellison JJ, McMurry TJ, Lauffer RB. Gadolinium(III) Chelates as MRI Contrast Agents: Structure, Dynamics, and Applications. Chem Rev. 1999; 99:2293–2352. [PubMed: 11749483]
- 9. Song Y, Zong H, Trivedi ER, Vesper BJ, Waters EA, Barrett AG, Radosevich JA, Hoffman BM, Meade TJ. Synthesis and Characterization of New Porphyrazine-Gd(III) Conjugates as Multimodal MR Contrast Agents. Bioconjugate Chem. 2010; 21:2267–2275.
- 10. Frullano L, Meade TJ. Multimodal MRI Contrast Agents. J Biol Iinorg Chem. 2007; 12:939–949.
- 11. Tu CQ, Louie AY. Photochromically-Controlled, Reversibly-Activated MRI and Optical Contrast Agent. Chem Commun. 2007:1331–1333.
- Uzgiris EE, Cline H, Moasser B, Grimmond B, Amaratunga M, Smith JF, Goddard G. Conformation and Structure of Polymeric Contrast Agents for Medical Imaging. Biomacromolecules. 2004; 5:54–61. [PubMed: 14715008]
- Endres PJ, MacRenaris KW, Vogt S, Meade TJ. Cell-Permeable MR Contrast Agents With Increased Intracellular Retention. Bioconjugate Chem. 2008; 19:2049–2059.
- Laurent S, Forge D, Port M, Roch A, Robic C, Vander Elst L, Muller RN. Magnetic Iron Oxide Nanoparticles: Synthesis, Stabilization, Vectorization, Physicochemical Characterizations, and Biological Applications. Chem Rev. 2008; 108:2064–2110. [PubMed: 18543879]
- Hu F, Macrenaris KW, Waters EA, Schultz-Sikma EA, Eckermann AL, Meade TJ. Highly Dispersible, Superparamagnetic Magnetite Nanoflowers for Magnetic Resonance Imaging. Chem Commun. 2010; 46:73–75.
- Cho SJ, Jarrett BR, Louie AY, Kauzlarich SM. Gold-Coated Iron Nanoparticles: A Novel Magnetic Resonance Agent for T-1 and T-2 Weighted Imaging. Nanotechnology. 2006; 17:640–644.
- Huber MM, Staubli AB, Kustedjo K, Gray MH, Shih J, Fraser SE, Jacobs RE, Meade TJ.
  Fluorescently Detectable Magnetic Resonance Imaging Agents. Bioconjugate Chem. 1998; 9:242–249.
- Hooker JM, Datta A, Botta M, Raymond KN, Francis MB. Magnetic Resonance Contrast Agents From Viral Capsid Shells: A Comparison of Exterior and Interior Cargo Strategies. Nano Lett. 2007; 7:2207–2210. [PubMed: 17630809]
- 19. Crich SG, Biancone L, Cantaluppi V, Duo D, Esposito G, Russo S, Camussi G, Aime S. Improved Route for The Visualization of Stem Cells Labeled With a Gd-/Eu-Chelate as Dual (MRI and Fluorescence) Agent. Magn Reson Med. 2004; 51:938–944. [PubMed: 15122675]
- 20. Brekke C, Morgan SC, Lowe AS, Meade TJ, Price J, Williams SC, Modo M. The *In Vitro* Effects of a Bimodal Contrast Agent on Cellular Functions and Relaxometry. NMR in Biomed. 2007; 20:77–89.
- 21. Anderson EA, Isaacman S, Peabody DS, Wang EY, Canary JW, Kirshenbaum K. Viral Nanoparticles Donning a Paramagnetic Coat: Conjugation of MRI Contrast Agents to the MS2 Capsid. Nano Lett. 2006; 6:1160–1164. [PubMed: 16771573]
- Santra S, Kaittanis C, Grimm J, Perez JM. Drug/Dye-Loaded, Multifunctional Iron Oxide Nanoparticles for Combined Targeted Cancer Therapy and Dual Optical/Magnetic Resonance Imaging. Small. 2009; 5:1862–1868. [PubMed: 19384879]
- Chen T, Shukoor MI, Wang R, Zhao Z, Yuan Q, Bamrungsap S, Xiong X, Tan W. Smart Multifunctional Nanostructure for Targeted Cancer Chemotherapy and Magnetic Resonance Imaging. ACS Nano. 2011; 5:7866–7873. [PubMed: 21888350]
- 24. Kim HM, Lee H, Hong KS, Cho MY, Sung MH, Poo H, Lim YT. Synthesis and High Performance of Magnetofluorescent Polyelectrolyte Nanocomposites as MR/Near-Infrared Multimodal Cellular Imaging Nanoprobes. ACS Nano. 2011; 5:8230–8240. [PubMed: 21932788]
- 25. Paquet C, de Haan HW, Leek DM, Lin HY, Xiang B, Tian G, Kell A, Simard B. Clusters of Superparamagnetic Iron Oxide Nanoparticles Encapsulated in a Hydrogel: A Particle Architecture

- Generating a Synergistic Enhancement of the T2 Relaxation. ACS Nano. 2011; 5:3104–3112. [PubMed: 21428441]
- 26. Poselt E, Kloust H, Tromsdorf U, Janschel M, Hahn C, Masslo C, Weller H. Relaxivity Optimization of a PEGylated Iron-Oxide-Based Negative Magnetic Resonance Contrast Agent for T(2)-Weighted Spin-Echo Imaging. ACS Nano. 2012; 6:1619–1624. [PubMed: 22276942]
- 27. Tromsdorf UI, Bigall NC, Kaul MG, Bruns OT, Nikolic MS, Mollwitz B, Sperling RA, Reimer R, Hohenberg H, Parak WJ, et al. Size and Surface Effects on the MRI Relaxivity of Manganese Ferrite Nanoparticle Contrast Agents. Nano Lett. 2007; 7:2422–2427. [PubMed: 17658761]
- Tu C, Ng TS, Sohi HK, Palko HA, House A, Jacobs RE, Louie AY. Receptor-Targeted Iron Oxide Nanoparticles for Molecular MR Imaging of Inflamed Atherosclerotic Plaques. Biomaterials. 2011; 32:7209–7216. [PubMed: 21742374]
- 29. Bae KH, Kim YB, Lee Y, Hwang J, Park H, Park TG. Bioinspired Synthesis and Characterization of Gadolinium-Labeled Magnetite Nanoparticles for Dual Contrast T(1)- and T(2)-Weighted Magnetic Resonance Imaging. Bioconjugate Chem. 2010; 21:505–512.
- 30. Bull SR, Guler MO, Bras RE, Meade TJ, Stupp SI. Self-Assembled Peptide Amphiphile Nanofibers Conjugated to MRI Contrast Agents. Nano Lett. 2005; 5:1–4. [PubMed: 15792402]
- 31. Bull SR, Guler MO, Bras RE, Venkatasubramanian PN, Stupp SI, Meade TJ. Magnetic Resonance Imaging of Self-Assembled Biomaterial Scaffolds. Bioconjugate Chem. 2005; 16:1343–1348.
- 32. Datta A, Hooker JM, Botta M, Francis MB, Aime S, Raymond KN. High Relaxivity Gadolinium Hydroxypyridonate-Viral Capsid Conjugates: Nanosized MRI Contrast Agents. J Am Chem Soc. 2008; 130:2546–2552. [PubMed: 18247608]
- Drake P, Cho HJ, Shih PS, Kao CH, Lee KF, Kuo CH, Lin XZ, Lin YJ. Gd-Doped Iron-Oxide Nanoparticles for Tumor Therapy via Magnetic Field Hyperthermia. J Mater Chem. 2007; 17:4914–4918.
- Pan D, Caruthers SD, Hu G, Senpan A, Scott MJ, Gaffney PJ, Wickline SA, Lanza GM. Ligand-Directed Nanobialys as Theranostic Agent for Drug Delivery and Manganese-Based Magnetic Resonance Imaging of Vascular Targets. J Am Chem Soc. 2008; 130:9186–9187. [PubMed: 18572935]
- 35. Song Y, Kohlmeir EK, Meade TJ. Synthesis of Multimeric MR Contrast Agents for Cellular Imaging. J Am Chem Soc. 2008; 130:6662–6663. [PubMed: 18452288]
- 36. Song Y, Xu X, MacRenaris KW, Zhang XQ, Mirkin CA, Meade TJ. Multimodal Gadolinium-Enriched DNA-Gold Nanoparticle Conjugates for Cellular Imaging. Angew Chem Int Ed Engl. 2009; 48:9143–9147. [PubMed: 19882611]
- Cheng Z, Thorek DL, Tsourkas A. Gadolinium-Conjugated Dendrimer Nanoclusters as a Tumor Targeted T1 Magnetic Resonance Imaging Contrast Agent. Angew Chem Int Ed Engl. 2010; 49:346–350. [PubMed: 19967688]
- 38. Cheng ZL, Thorek DLJ, Tsourkas A. Porous Polymersomes With Encapsulated Gd-Labeled Dendrimers as Highly Efficient MRI Contrast Agents. Adv Funct Mater. 2009; 19:3753–3759.
- 39. Allen MJ, MacRenaris KW, Venkatasubramanian PN, Meade TJ. Cellular Delivery of MRI Contrast Agents. Chemistry & Biology. 2004; 11:301–307. [PubMed: 15123259]
- Manus LM, Mastarone DJ, Waters EA, Zhang XQ, Schultz-Sikma EA, Macrenaris KW, Ho D, Meade TJ. Gd(III)-Nanodiamond Conjugates for MRI Contrast Enhancement. Nano Lett. 2010; 10:484–489. [PubMed: 20038088]
- 41. Mastarone DJ, Harrison VS, Eckermann AL, Parigi G, Luchinat C, Meade TJ. A Modular System for the Synthesis of Multiplexed Magnetic Resonance Probes. J Am Chem Soc. 2011; 133:5329–5337. [PubMed: 21413801]
- 42. Major JL, Meade TJ. Bioresponsive, Cell-Penetrating, and Multimeric MR Contrast Agents. Acc Chem Res. 2009; 42:893–903. [PubMed: 19537782]
- 43. Kalman FK, Woods M, Caravan P, Jurek P, Spiller M, Tircso G, Kiraly R, Brucher E, Sherry AD. Potentiometric and Relaxometric Properties of a Gadolinium-Based MRI Contrast Agent for Sensing Tissue pH. Inorg Chem. 2007; 46:5260–5270. [PubMed: 17539632]
- 44. Duimstra JA, Femia FJ, Meade TJ. A Gadolinium Chelate for Detection of Beta-Glucuronidase: a Self-Immolative Approach. J Am Chem Soc. 2005; 127:12847–12855. [PubMed: 16159278]

45. Caravan P, Cloutier NJ, Greenfield MT, McDermid SA, Dunham SU, Bulte JW, Amedio JC Jr, Looby RJ, Supkowski RM, Horrocks WD, et al. The Interaction of MS-325 With Human Serum Albumin and Its Effect on Proton Relaxation Rates. J Am Chem Soc. 2002; 124:3152–3162. [PubMed: 11902904]

- 46. Caravan P. Strategies for Increasing the Sensitivity of Gadolinium Based MRI Contrast Agents. Chem Soc Rev. 2006; 35:512–523. [PubMed: 16729145]
- 47. Aime S, Castelli DD, Crich SG, Gianolio E, Terreno E. Pushing the Sensitivity Envelope of Lanthanide-Based Magnetic Resonance Imaging (MRI) Contrast Agents for Molecular Imaging Applications. Acc Chem Res. 2009; 42:822–831. [PubMed: 19534516]
- 48. Tu C, Osborne EA, Louie AY. Activatable T1 and T2 Magnetic Resonance Imaging Contrast Agents. Ann Biomed Eng. 2011; 39:1335–1348. [PubMed: 21331662]
- 49. Major JL, Parigi G, Luchinat C, Meade TJ. The Synthesis and *In Vitro* Testing of a Zinc-Activated MRI Contrast Agent. Proc Natl Acad Sci US A. 2007; 104:13881–13886.
- Zhang XA, Lovejoy KS, Jasanoff A, Lippard SJ. Water-Soluble Porphyrins as a Dual-Function Molecular Imaging Platform for MRI and Fluorescence Zinc Sensing. Proc Natl Acad Sci US A. 2007; 104:10780–10785.
- Louie AY, Huber MM, Ahrens ET, Rothbacher U, Moats R, Jacobs RE, Fraser SE, Meade TJ. *In Vivo* Visualization of Gene Expression Using Magnetic Resonance Imaging. Nat Biotechnol. 2000; 18:321–325. [PubMed: 10700150]
- 52. Urbanczyk-Pearson LM, Meade TJ. Preparation of Magnetic Resonance Contrast Agents Activated by Beta-Galactosidase. Nat Protoc. 2008; 3:341–350. [PubMed: 18323804]
- Frullano L, Tejerina B, Meade TJ. Synthesis and Characterization of a Doxorubicin-Gd(III) Contrast Agent Conjugate: A New Approach Toward Prodrug-Procontrast Complexes. Inorg Chem. 2006; 45:8489–8491. [PubMed: 17029358]
- 54. Lee J, Burdette JE, MacRenaris KW, Mustafi D, Woodruff TK, Meade TJ. Rational Design, Synthesis, and Biological Evaluation of Progesterone-Modified MRI Contrast Agents. Chemistry & Biology. 2007; 14:824–834. [PubMed: 17656319]
- 55. Yang H, Zhuang Y, Sun Y, Dai A, Shi X, Wu D, Li F, Hu H, Yang S. Targeted Dual-Contrast T1-and T2-Weighted Magnetic Resonance Imaging of Tumors Using Multifunctional Gadolinium-Labeled Superparamagnetic Iron Oxide Nanoparticles. Biomaterials. 2011; 32:4584–4593. [PubMed: 21458063]
- Perez JM, Josephson L, O'Loughlin T, Hogemann D, Weissleder R. Magnetic Relaxation Switches Capable of Sensing Molecular Interactions. Nat Biotechnol. 2002; 20:816–820. [PubMed: 12134166]
- 57. Kaittanis C, Boukhriss H, Santra S, Naser SA, Perez JM. Rapid and Sensitive Detection of an Intracellular Pathogen in Human Peripheral Leukocytes With Hybridizing Magnetic Relaxation Nanosensors. PloS One. 2012; 7:e35326. [PubMed: 22496916]
- Kaittanis C, Santra S, Perez JM. Role of Nanoparticle Valency in the Nondestructive Magnetic-Relaxation-Mediated Detection and Magnetic Isolation of Cells in Complex Media. J Am Chem Soc. 2009; 131:12780–12791. [PubMed: 19681607]
- Kaittanis C, Santra S, Santiesteban OJ, Henderson TJ, Perez JM. The Assembly State Between Magnetic Nanosensors and Their Targets Orchestrates Their Magnetic Relaxation Response. J Am Chem Soc. 2011; 133:3668–3676. [PubMed: 21341659]
- 60. Haun JB, Castro CM, Wang R, Peterson VM, Marinelli BS, Lee H, Weissleder R. Micro-NMR for Rapid Molecular Analysis of Human Tumor Samples. SciTrans Med. 2011; 3:71ra16.
- Asati A, Santra S, Kaittanis C, Nath S, Perez JM. Oxidase-Like Activity of Polymer-Coated Cerium Oxide Nanoparticles. Angew Chem Int Ed Engl. 2009; 48:2308–2312. [PubMed: 19130532]
- Asati A, Santra S, Kaittanis C, Perez JM. Surface-Charge-Dependent Cell Localization and Cytotoxicity of Cerium Oxide Nanoparticles. ACS Nano. 2010; 4:5321–5331. [PubMed: 20690607]
- Santra S, Kaittanis C, Perez JM. Aliphatic Hyperbranched Polyester: A New Building Block in the Construction of Multifunctional Nanoparticles and Nanocomposites. Langmuir. 2010; 26:5364– 5373. [PubMed: 19957939]

64. Lattuada L, Lux G. Synthesis of Gd-DTPA-Cholesterol: A New Lipophilic Gadolinium Complex as a Potential MRI Contrast Agent. Tetrahedron Lett. 2003; 44:3893–3895.

- 65. Weinmann HJ, Brasch RC, Press WR, Wesbey GE. Characteristics of Gadolinium-DTPA Complex: A Potential NMR Contrast Agent. Am J Roentgenol. 1984; 142:619–624. [PubMed: 6607655]
- 66. McCarthy JR, Perez JM, Bruckner C, Weissleder R. Polymeric Nanoparticle Preparation That Eradicates Tumors. Nano Lett. 2005; 5:2552–2556. [PubMed: 16351214]
- 67. Sun EY, Josephson L, Weissleder R. "Clickable" Nanoparticles for Targeted Imaging. Mol Imaging. 2006; 5:122–128. [PubMed: 16954026]
- 68. Perez JM, Asati A, Nath S, Kaittanis C. Synthesis of Biocompatible Dextran-Coated Nanoceria With pH-Dependent Antioxidant Properties. Small. 2008; 4:552–556. [PubMed: 18433077]

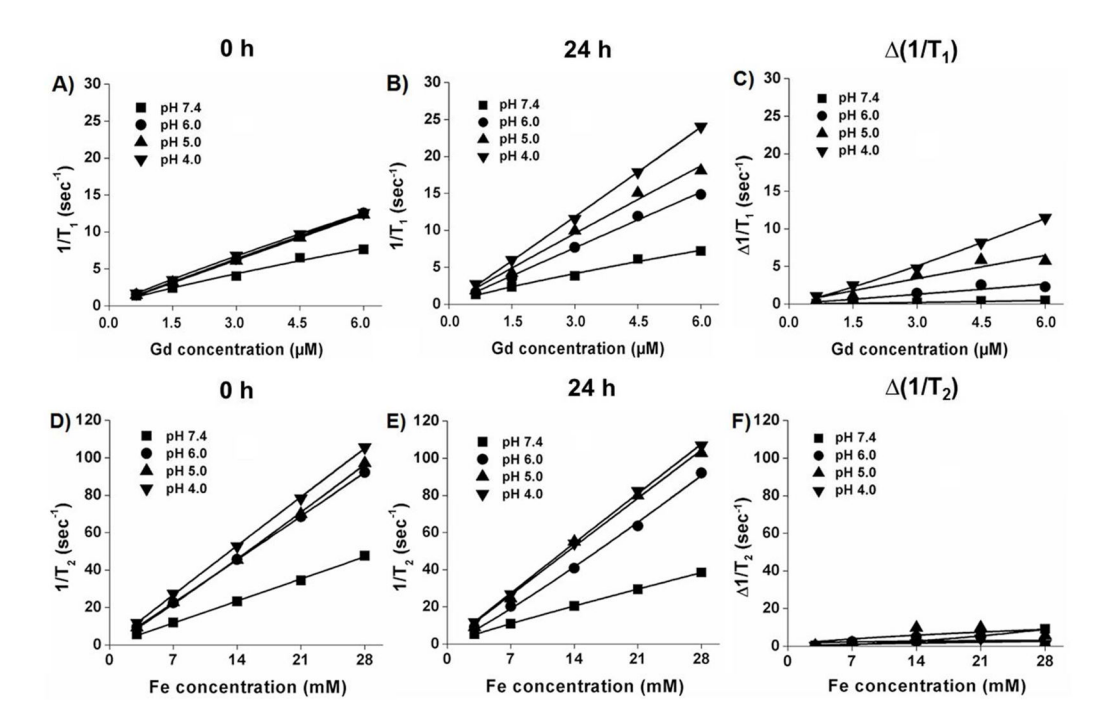


Figure 1. Assessment of magnetic relaxations of activatable magnetic nanoprobe IO-PAA-Gd-DTPA using bench-top magnetic relaxometer (Bruker's Minispec, B = 0.47 T). Inverse spin-lattice  $(1/T_I)$  and spin-spin  $(1/T_2)$  magnetic relaxation times were measured before and after 24 h of incubation in different PBS solutions (pH = 4.0–7.4, 37 °C) and at different nanoprobe concentrations. (A) Initial  $1/T_I$  measurements right after the addition of PBS solutions, (B)  $1/T_I$  measurements after 24 h of incubation, (C) the differential  $1/T_I$  values prior to and after incubation. (D) Initial  $1/T_2$  measurements right after the addition of PBS solutions, (E)  $1/T_2$  measurements after 24 h of incubation, (F) the differential  $1/T_2$  values prior to and after incubation. (Means  $\pm$  SE; SE were within 1–4%, which are too small to be depicted).

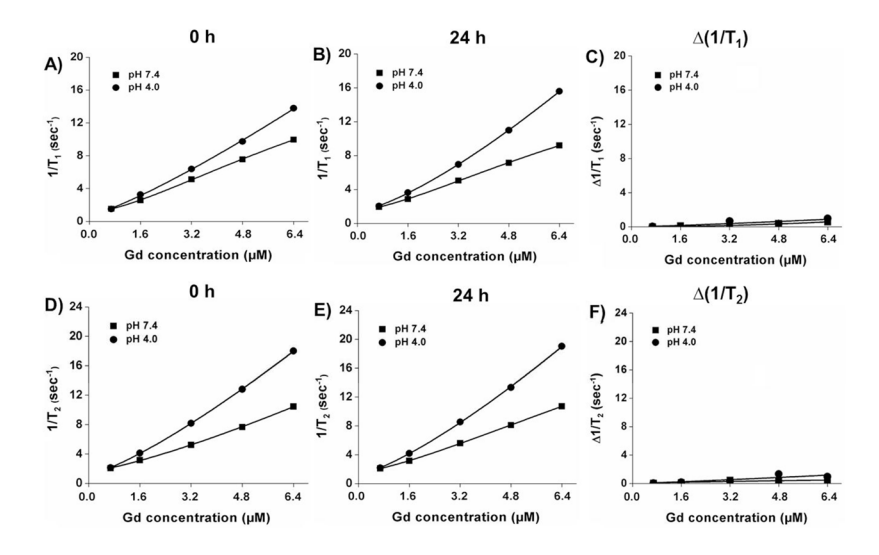


Figure 2. Assessment of magnetic relaxations of composite nanoceria NC-PAA-Gd-DTPA using bench-top magnetic relaxometer (Bruker's Minispec, B = 0.47 T). Inverse spin-lattice ( $1/T_I$ ) and spin-spin ( $1/T_2$ ) magnetic relaxation times were measured before and after 24 h of incubation in different PBS solutions (pH = 4.0 and 7.4, 37 °C) and at different nanoprobe concentrations. (A) Initial  $1/T_I$  measurements right after the addition of PBS solutions, (B)  $1/T_I$  measurements after 24 h of incubation and (C) the differential  $1/T_I$  values prior to and after incubation. (D) Initial  $1/T_2$  measurements right after the addition of PBS solutions, (E)  $1/T_2$  measurements after 24 h of incubation and (F) the differential  $1/T_2$  values prior to and after incubation. (Means  $\pm$  SE; SE were within 1-4%, which are too small to be depicted).

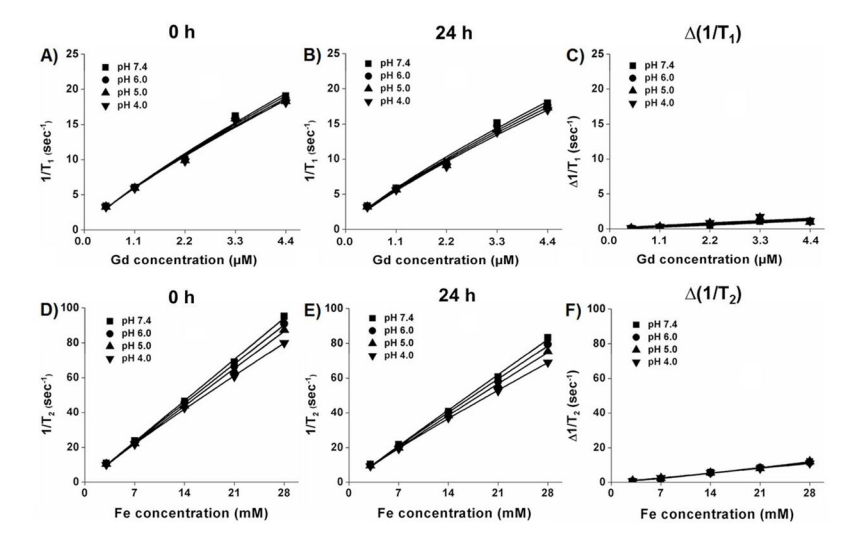


Figure 3. Assessment of magnetic relaxations of Gd-DTPA surface conjugating IO-PAA magnetic nanoprobes, using bench-top magnetic relaxometer (Bruker's Minispec, B = 0.47 T). Inverse spin-lattice  $(1/T_I)$  and spin-spin  $(1/T_2)$  magnetic relaxation times were measured before and after 24 h of incubation in different PBS solutions (pH = 4.0–7.4, 37 °C) and at different nanoprobe concentrations. (A) Initial  $1/T_I$  measurements right after the addition of PBS solutions, (B)  $1/T_I$  measurements after 24 h of incubation and (C) the differential  $1/T_I$  values prior to and after incubation. (D) Initial  $1/T_2$  measurements right after the addition of PBS solutions, (E)  $1/T_2$  measurements after 24 h of incubation and (F) the differential  $1/T_2$  values prior to and after incubation. (Means  $\pm$  SE; SE were within 1–4%, which are too small to be depicted).

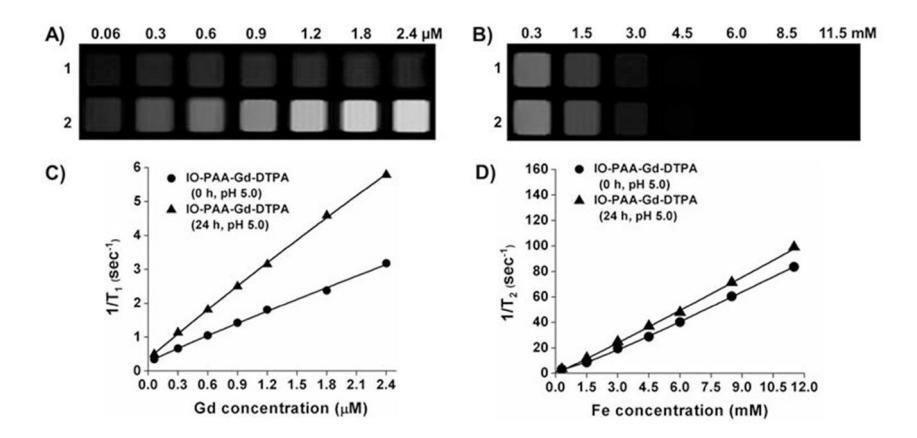


Figure 4. Magnetic Resonance Imaging (MRI) studies measuring the magnetic activations (TI- and T2- Map) of our activatable magnetic IO-PAA-Gd-DTPA nanoprobes in PBS at pH 5.0. (A)  $T_I$ -weighted MRI images of increasing Gd concentrations (0.06  $\mu$ M-2.4  $\mu$ M) of IO-PAA-Gd-DTPA nanoprobes prior to (1) and after 24 h of incubation (2) at 37 °C, (B)  $T_2$ -weighted MRI images of increasing Fe concentrations (0.3 mM-11.5 mM) of IO-PAA-Gd-DTPA nanoprobes prior to (1) and after 24 h of incubation (2) at 37 °C, (C) Corresponding  $1/T_I$  relaxation rates prior to ( $\blacksquare$ ) and after ( $\blacksquare$ ) 24 h of incubation, (D) Corresponding  $1/T_2$  relaxation rate prior to ( $\blacksquare$ ) and after ( $\blacksquare$ ) 24 h of incubation. (Means  $\pm$  SE; SE were within 1–4%, which are too small to be depicted).

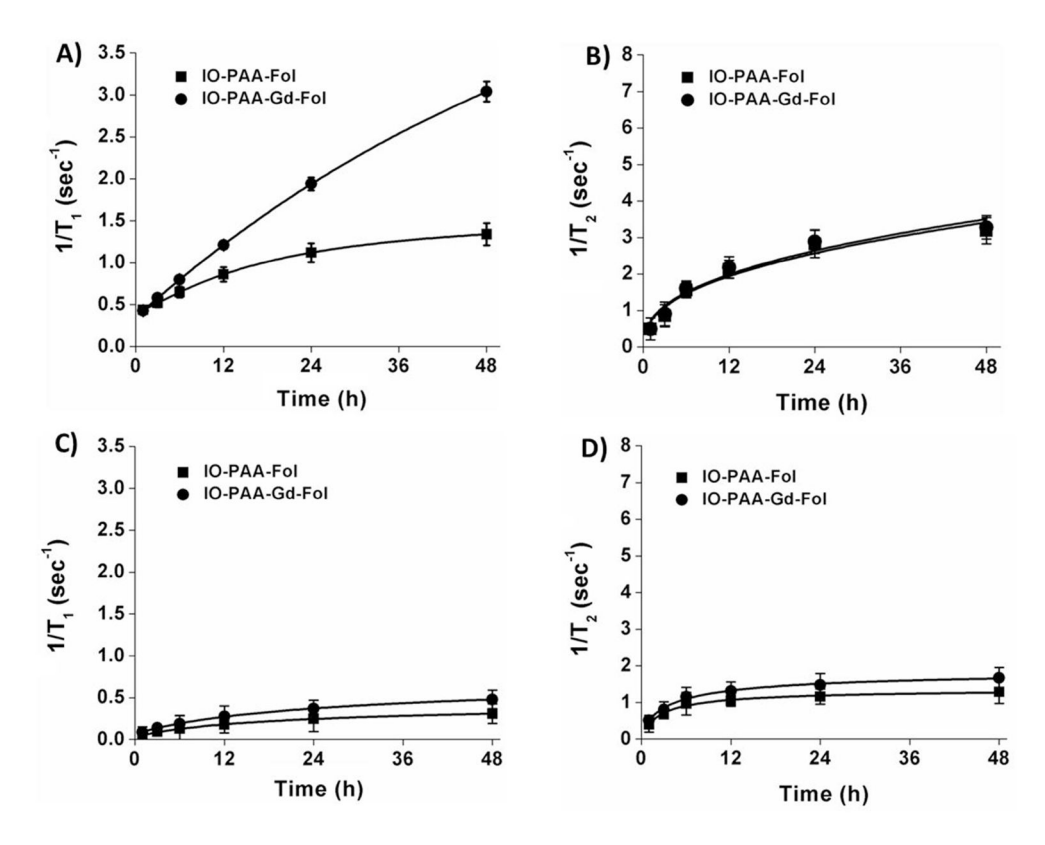
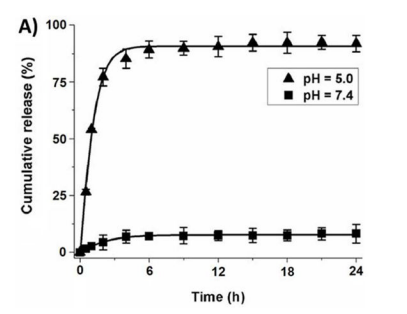


Figure 5. Intracellular magnetic activations of our folate-decorated activatable IO-PAA-Gd-DTPA-Fol nanoprobe ( $\P$ ,100  $\mu$ L, 28 mM) and the control IO-PAA-Fol nanoprobe ( $\P$ ,100  $\mu$ L, 28 mM) using FR-expressing HeLa cells (A and B) and FR-negative H9c2 cells (C and D). Significant activation in inverse spin-lattice magnetic relaxations ( $1/T_I$ ) was observed from HeLa cells incubated with the activatable IO-PAA-Gd-DTPA-Fol nanoprobes ( $\P$ , Figure 5A). As expected, no significant changes in  $1/T_2$  were observed from HeLa cells due to absence of any  $T_2$  activations (Figure 5B). Neither  $1/T_I$  (Figure 5C) nor  $1/T_2$  (Figure 5D) activations were observed from H9c2 cells due to lack of any receptor-mediated internalizations.



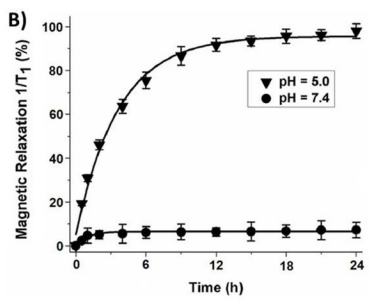


Figure 6. Rate of release of taxol and Gd-DTPA at 37 °C. A) HPLC experiment ( $\lambda_{abs} = 227$  nm) indicated the time-dependent release of taxol from the activatable IO-PAA-Gd-DTPA nanoprobes (50  $\mu$ L, 28 mM) when incubated at pH = 5.0 ( $\blacktriangle$ ) solution. No significant release of taxol was observed ( $\blacksquare$ ) when incubated in PBS at pH 7.4. B) The observed increase rate of taxol release was accompanied by a gradual increase in the inverse spinlattice magnetic relaxation ( $1/T_I$ ) recorded using magnetic relaxometer ( $\blacktriangledown$ , B = 0.47 T, pH = 5.0). As expected, nominal increase in the inverse spin-lattice magnetic relaxation ( $\blacksquare$ , 1/ $T_I$ ) was observed when incubated in PBS at pH = 7.4.

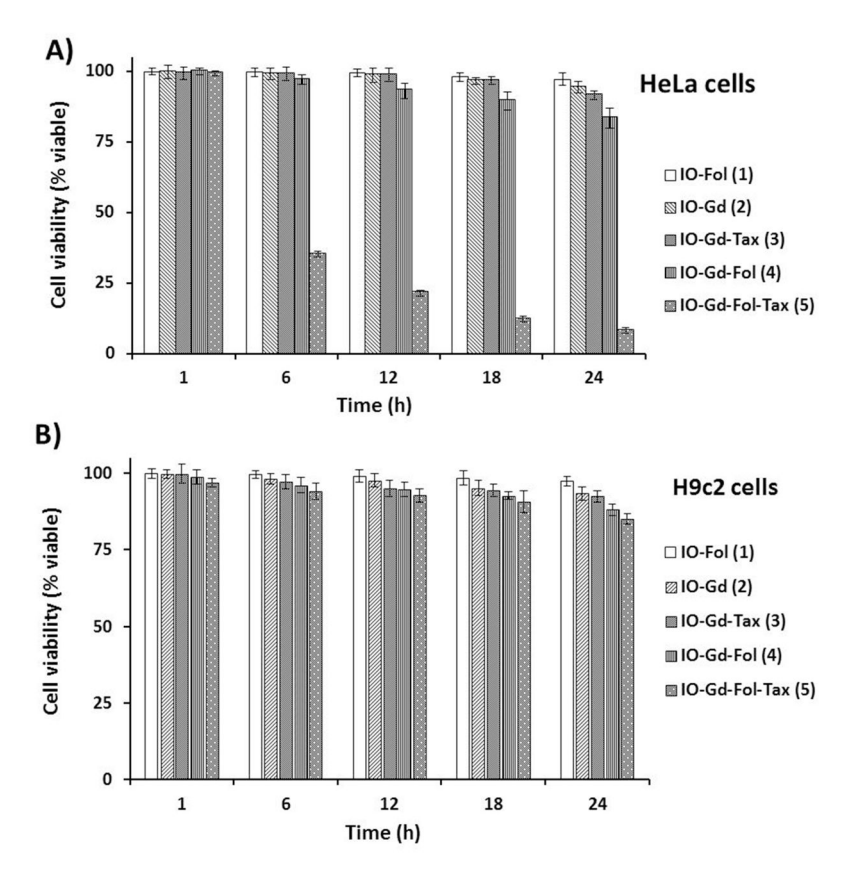
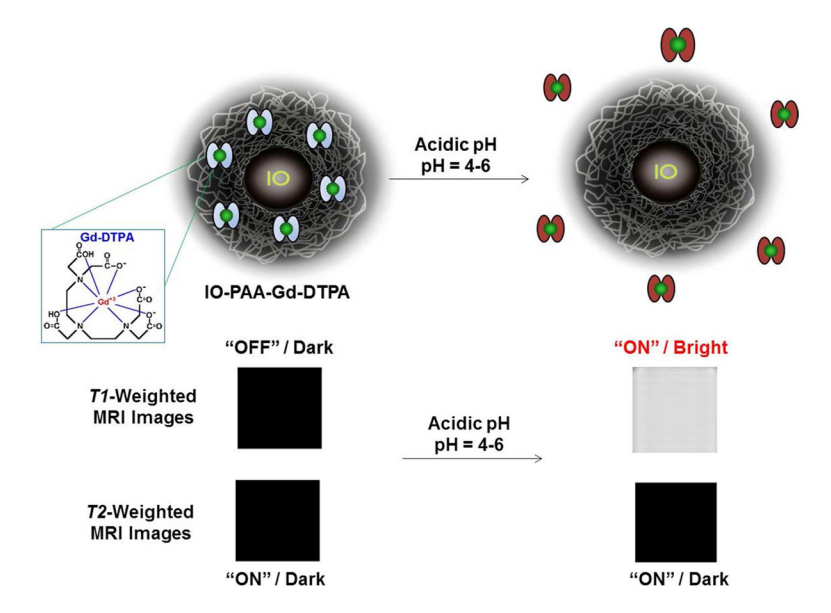


Figure 7. In Vitro cytotoxicity of taxol-encapsulating activatable IO-PAA-Gd-DTPA nanoprobes. Time-dependent in vitro MTT assays for the determination of cytotoxicity of the functional magnetic nanoprobes (1–5, 35  $\mu$ L, 28 mM in PBS pH = 7.4). HeLa cells (A) and H9c2 cells (B) treated with the functional magnetic nanoprobes. Folate-conjugated (1), Gd-DTPA encapsulating (2), Gd-DTPA and taxol-encapsulating (3) magnetic nanoprobes showed biocompatibility with nominal toxicity in both the cell lines. The Gd-DTPA encapsulating folate-conjugated magnetic nanoprobes (4) showed more than 15% reduction in cell viability, whereas Gd-DTPA and taxol encapsulating folate-conjugated magnetic nanoprobes (5) showed more than 90% reduction in cell viability when treated with HeLa cells (A) and not with H9c2 cells (B), confirming the folate-receptor mediated internalizations and ability for targeted therapy. Average values of four measurements are depicted  $\pm$  standard errors.



### Scheme 1.

Schematic representation of the acidic pH-mediated activation of the activatable composite magnetic nanoprobe IO-PAA-Gd-DTPA and corresponding  $T_I$ -MR activation. In an acidic environment, the quenched Gd-DTPA chelates are released from the iron oxide's (IO) polymeric coating becoming activated (ON) and resulting in an enhancement in the T1-weighted MRI image (brighter signal) and no change in the T2-weighted image.

Santra et al.

Table 1

Magnetic relaxation values at 0.47 T of the nanocomposite based on Gd concentrations at different pH.

Nanoprobe	hН	$r_I \; (\mathrm{mM}^{-1}\mathrm{Sec}^{-1})$	pH $r_I$ (mM <sup>-1</sup> Sec <sup>-1</sup> ) $r_2$ (mM <sup>-1</sup> Sec <sup>-1</sup> ) % Change $r_I$	% Change $r_I$	% Change $r_2$
IO-PAA-Gd-DTPA (Encapsulated)	7.4	$50.2\pm1.8$	87.3±2.4		-
[Gd] = 0.289 mg/mL	6.0	72.5±1.3	98.2±3.2	44	12
	5.0	84.3±1.2	111.6±2.8	89	28
	4.0	97.0±2.5	118.5±3.4	66	38
IO-PAA-Gd-DTPA (Surface)	7.4	63.4±1.5	92.1±3.8		1
[Gd] = 0.201  mg/mL	6.0	66.3±2.2	95.2±1.2	5	3
	5.0	68.1±1.4	97.4±2.1	L	9
	4.0	69.3±1.3	98.5±1.8	6	7

Page 25